Advanced Steel Construction – Vol. 18 No. 1 (2022) 425–435
DOI:10.18057/IJASC.2022.18.1.1

BUCKLING BEHAVIOR OF A WHEEL COUPLER HIGH-FORMWORK SUPPORT SYSTEM BASED ON SEMI-RIGID CONNECTION JOINTS

Jin-Feng Dong, Hai-Qing Liu and Zhong-Wei Zhao *

School of Civil Engineering, Liaoning Technical University, Fuxin 123000, China
** (Corresponding author: E-mail: zhaozhongwei@lntu.edu.cn)*

ABSTRACT

To clarify the buckling behavior of a wheel coupler high-formwork support system with a diagonal bracing, the positive and negative bending behaviors of the connection joints of the support were systematically studied through experiments. Through a parametric analysis and a finite element analysis, a precise numerical model of the connection joints of the wheel coupler was established and verified. Based on the characteristics of the semi-rigid connections, the buckling behavior of the overall structure was analyzed. The results showed that the failure modes in the positive direction were correlated with the insertion depth of the socket into the template; the greater the depth, the more likely the socket was to fracture. The failure modes in the negative direction were closely related to the insertion depth and the bending of the vertical post. An appropriate joint density was conducive to the overall stability. In the presence of a lateral constraint at the top, the greater the angle between the diagonal bracing and the horizontal plane, the better the overall stability under the same joint density. The optimal layout of the vertical diagonal bracing was a 2-span, 4-step arrangement, and the optimal angle was in the range of 30–70°. In the absence of a lateral constraint at the top, the smaller the angle between the diagonal bracing and the horizontal plane, the better the overall stability under the same joint density. The optimal angle was approximately 30° when the lift height was moderate.

ARTICLE HISTORY

Received: 5 December 2020
Revised: 21 May 2021
Accepted: 24 May 2021

KEYWORDS

Semi-rigid connection joints;
Wheel coupler high-formwork support system;
Diagonal bracing;
Buckling behavior

1. Introduction

Wheel coupler formwork supports have been widely used in construction to support the gravity load of floor slabs. However, the reliability of their mechanical behavior has not been sufficiently studied. Existing results are mostly applicable to conventional fastener-type and bowl buckle-type formwork supports [1-3], which are not widely used as external scaffolds or formwork supports. Dou et al. [4] and Chen [5] investigated and analyzed a socket-type wheel coupler formwork support, they concluded that this support can be considered an extended version of the socket-type disc-buckle formwork support. However, the design, production, and construction of such a support cannot be implemented in accordance with the construction specification employed for disc-buckle formwork supports because of the differences in terms of the structure and calculation parameters. No relevant product standards or technical specifications have been issued. We refer to the "Safety technical specification for wheel-coupler steel pipe scaffold" issued by Guangdong Province, China [6]. Therefore, further research on the behavior aspects should be conducted.

The mechanical behavior of the connection joints of formwork supports is complex because of the need for a rapid assembly during construction. The semi-rigid joints significantly influence the bearing capacity of the overall formwork support system [7-10]. There are many studies on semi-rigid joints of steel frames [11-20]. In the classic design and calculation theory of steel structures [21], the joint between a steel frame beam and a column is considered a rigid joint or a hinge joint. The calculations in this simplified method can be easily implemented. However, it cannot reflect the true stress state of the overall structure. Therefore, it is necessary to study the semi-rigid joints of wheel coupler-type steel pipe formwork support systems, because the joint is semi-rigid in theory, mainly including the influences of joint stiffness and geometrical imperfections on the overall stability.

Current studies have mostly focused on the joints of fastener-type formwork supports [22, 23]. The results have shown that the ultimate bearing capacity of fastener-type formwork systems increases nonlinearly with the increase in the semi-rigid value. For a bowl buckle-type joint, Zou et al. [24] found that a trilinear semi-rigid joint model provides a reliable accuracy and is suitable for a refined numerical simulation of bowl buckle-type formwork supports. The bearing capacity increases with the increase in the initial bending stiffness and presents a three-stage variation. Compared with the joint stiffness of the conventional fastener-type steel pipe formwork support, the stiffness range of the connection joints of a wheel coupler formwork support varies [25], and the spacing and lift height of the vertical post significantly influence the overall stability. Yu et al. [26] and Chu et al. [27] integrated the lowest eigenmode with a column out-of-straightness magnitude of 1/1000 for the height of the scaffold units into the model. Sevim et al. [28] investigated the effects of truss height and number of tie bars on the structural behavior of suspended scaffolding systems through experiments, the results showed that a scaffolding system with 60 cm-high truss and two tie bars presents optimal safety and cost-savings. Liu et al. [29] presented a mortise–tenon steel-tube scaffold, the influencing laws of storey height, vertical member interval and other factors were determined through parameter analysis, research results provide important references for future in-depth studies and engineering applications of the mortise–tenon steel-tube scaffold.

In this work, the connection joints of a wheel coupler formwork support were studied through experiments and numerical analyses. The bending stiffness of the joints was obtained on the basis of the connection characteristics of semi-rigid joints. Fine connection joints were established using nonlinear spring elements, and the joint stiffness data were based on the experiment. A complete nonlinear buckling analysis and a first-mode buckling analysis were carried out on the numerical model of the wheel coupler high-formwork support system with a diagonal bracing. With this, we study the selection of the spatial layout of the diagonal bracing and the influences of the plane layout of the vertical diagonal bracing, the joint density between the diagonal bracing and the frame, and the angle between the diagonal bracing and the horizontal plane on the overall stability of the wheel coupler high-formwork support system. Thus, our study provides a reference for the practical applications of wheel coupler formwork supports.

2. Experimental research on flexural behavior of socket connections

2.1. Experimental survey

2.1.1. Geometrical size of socket connection

Fig. 1 illustrates the components of the socket connection, which comprises a socket and a template, wherein the socket is welded to the end of a horizontal bar, and the template is welded to a vertical post. The horizontal bar, vertical post, and template were made of Q235, and the socket was made of cast steel given its complex shape and material properties.

(a) A socket connection joint

(b) Horizontal bar

(c) Socket connection zone

Fig. 1 Formwork support connection and composition diagram

Fig. 2 shows the geometrical dimensions of the socket connection of the wheel coupler formwork support adopted in our actual project. The outer diameter of the horizontal bar and the vertical post was set to 48 mm, and the thickness was set to 3.0 mm. Figs. 2(a) and 2(b) show the detailed geometrical dimensions of the socket. The thickness was set to 7 mm, and the size of the insertion hole on the template was 14 mm × 25 mm, as shown in Fig. 2(c).

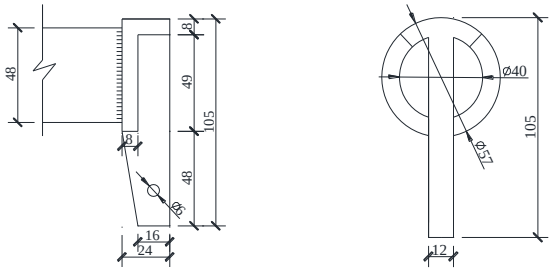

(a) Side view of the socket (b) Front view of the socket

(c) Template

Fig. 2 Geometrical dimensions of connection joints (all the dimensions in the figure are in mm).

The experimental specimen material was obtained from a construction site. The sizes of each group of experimental connection joints were different because of manufacturing errors. Fig. 3 shows the schematic of the socket insertion state.

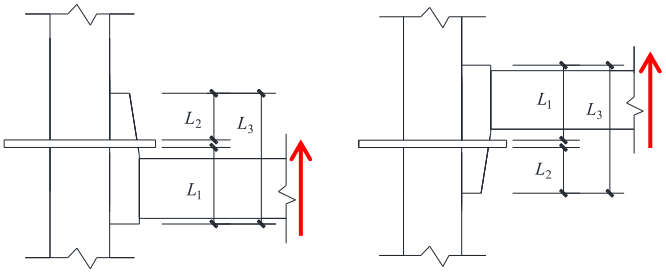

(a) Positive direction (b) Negative direction

Fig. 3 Schematic of the socket insertion state

Table 1 lists the detailed dimensions of the specimens. The letters prefixed to the specimen number indicate the loading direction, with "P'' representing a positive loading direction and "N" representing a negative loading direction. The positive loading results in a bending on the upper side of the horizontal bar, whereas the negative loading results in a compression.

Table 1
Detailed dimensions of the specimens

Specimen No.	L_1/mm	L_2/mm	L_3/mm
P-SJ1	66	30	103.0
P-SJ2	72	25	104.0
P-SJ3	73	23	103.0
P-SJ4	78	19	104.0
N-SJ1	71	26	103.0
N-SJ2	68	28	102.5
N-SJ3	62	34	104.0
N-SJ4	63	32	102.0

2.1.2. Experimental equipment and arrangement of the measuring points

Four 100 mm displacement transducers and one 200 mm displacement transducer were used to measure the displacement of the horizontal bar and the vertical post during the loading process. The distance between the upper and lower measuring points of the vertical post and the center of the joint was set to 150 mm, which were recorded as measuring point 1 and measuring point 2. The distances between the measuring point at the proximal end of the horizontal bar and the center of the joint were 85 mm and 185 mm, respectively, which were recorded as measuring points 3 and 4. The distance between the loading point at the far end of the horizontal bar and the joint center was set to 300 mm, which were recorded as measuring point 5 and used for data calibration. Fig. 4 shows the specific arrangement of the measuring points. ①~④ represent flange components.

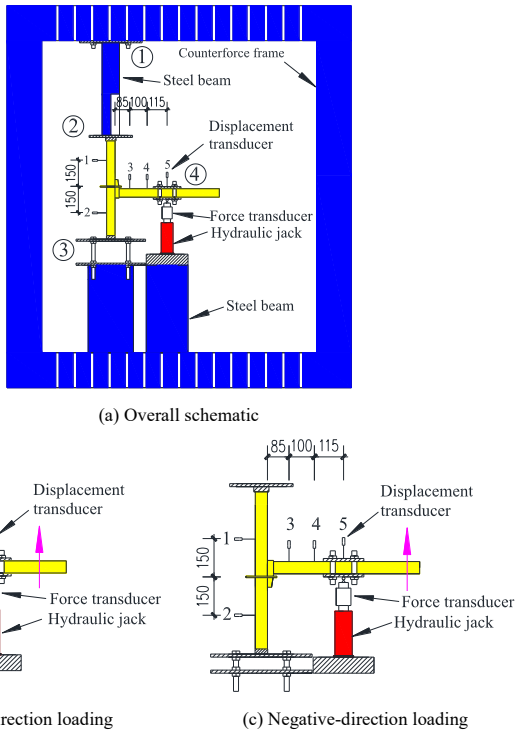

(a) Overall schematic

(b) Positive-direction loading (c) Negative-direction loading

Fig. 4 Experimental equipment and arrangement of the measuring points

2.1.3. Measurement method of joint rotational stiffness

Qian [30] employed the bending moment–rotation angle curve to measure the relevant parameters of disc-buckle type and bowl buckle-type formwork support joints. In this approach, the joint bending moment is taken as the product of the vertically concentrated load at the loading point of the horizontal bar and the distance from the loading point to the joint center, which can be calculated using Eq. (1), where F represents the vertically concentrated load at the loading point of the horizontal bar, and L represents the distance from the loading point to the joint center, which can be taken as 300 mm. The relative rotation angle of the joint can be obtained using Eq. (2). Here, Δ_1, Δ_2, Δ_3, and

Δ_4 respectively represent the displacement transducer reading data at measuring points 1, 2, 3, and 4, d_{3-4} represents the straight-line distance between the measuring points 3 and 4, d_1 and d_2 represent the distances from the measuring points 1 and 2 to the joint center, respectively, and θ_1 represents the rotation angle of the horizontal bar section relative to the joint. A section of the vertical post will produce a rotation angle relative to the joint, which is denoted by θ_2 and expressed in Eq. (2). After the influence of the deformation of the vertical post was compensated, the angle of the joint obtained was more accurate because the vertical post will also produce an elastic deformation during the loading process.

$$M = F \times L \tag{1}$$

$$\theta = \theta_1 - \theta_2 = \tan^{-1}\frac{\Delta_4 - \Delta_3}{d_{3-4}} - \tan^{-1}\frac{\Delta_2 - \Delta_1}{d_1 + d_2} \tag{2}$$

The bending moment–rotation angle curve of the joint was obtained by processing the data obtained from the experiment through Eqs. (1) and (2).

Fig. 5 shows the mechanical calculation model of the moment–rotation angle.

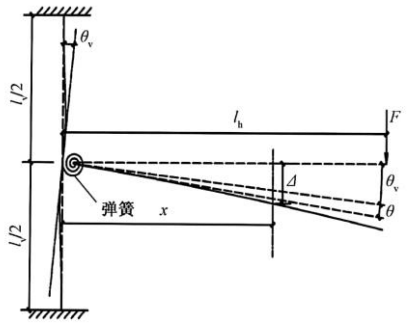

Fig. 5 Mechanical calculation model of moment–rotation angle

The vertical bending stiffness of the joint of the wheel coupler in an arbitrary stress state can be expressed as follows:

$$k = \frac{dM(\theta)}{d\theta} \tag{3}$$

The small deformation assumption is adopted to ignore the influence of component deformation on the component size. Under a vertically concentrated load, the vertical bending moment of the joint of the wheel coupler can be expressed as follows:

$$M = FL_h \tag{4}$$

Under the action of vertical bending moment, the rotation angle of the vertical pole at the joint of the wheel coupler can be expressed as follows:

$$\theta_v = \frac{ML_v}{16E_vI_v} \tag{5}$$

The spring rotation angle of the joint of the wheel coupler can be expressed as follows:

$$\theta = \frac{M}{k} \tag{6}$$

The relationship between the spring rotation angle of the joint of the wheel coupler, the vertical bending stiffness of the joint of the wheel coupler, and the vertical displacement at the measuring point is as follows:

$$(\theta_v + \theta)x + \frac{FL_hx^2}{2E_hI_h} - \frac{Fx^3}{6E_hI_h} = \Delta \tag{7}$$

By substituting (4) and (5) into (7), the relationship between the vertical bending moment and the rotation angle can be obtained:

$$M = \frac{48E_hE_vI_hI_vL_h(\Delta - \theta x)}{3E_hI_hL_hL_vx + 8E_vI_vx^2(3L_h - x)} \tag{8}$$

Here, k represents the vertical bending stiffness of the joint, $dM(\theta)$ represents the vertical bending stiffness increment of the joint, $d\theta$ represents the angle increment of the spring joint, M represents the vertical bending moment of the joint, F represents the vertically concentrated load at the loading point of the horizontal bar, L_h represents the distance between the loading point of the vertically concentrated load of the horizontal bar and the axis line of the vertical pole, θ_v represents the angle of the vertical pole at the joints, and L_v represents the length of the vertical pole, E_v represents the elastic modulus of the vertical pole, I_v represents the cross-sectional moment of inertia of the vertical pole; θ represents the spring angle of the joint, x represents the distance between the measuring point of the vertical displacement on the horizontal bar and the axis line of the vertical pole, E_h represents the elastic modulus of the horizontal bar, I_h represents the cross-sectional moment of inertia of the horizontal bar, and Δ represents the measured vertical displacement of the horizontal bar.

From Eq. (8), we find that the position of the measuring point has little influence on the bending moment–rotation angle of the joint, and the influence degree is not in the same order of magnitude.

2.1.4. Loading mechanism

The loading point was set 300 mm away from the joint on the horizontal bar, and a uniaxial loading was applied using a hydraulic jack. The loading force data were read using a force transducer connected to a computer. The experimental process included preloading, formal loading, and unloading. The step loading was carried out in the way of force control. There were four groups of parallel experiments. The loading in each step was 1/10-1/15 of the estimated ultimate load, and the load was kept in each step for 2 min. When the horizontal bar had a large rotation angle relative to the vertical post, we observed the deformation of the joint and the steel tube; the load did not increase, but the displacement continued to increase. At this point, we considered that the joint reached the ultimate failure state, and the loading was stopped. Tables 2 and 3 list the positive and negative loading mechanisms, respectively.

Table 2
Positive-direction experimental loading mechanism

Loading force /kN	0.2	0.4	...	1.4	1.6	1.7	1.8	...
Load keeping time /min	2	2	...	2	2	2	2	...

Table 3
Negative-direction experimental loading mechanism

Loading force/kN	0.7	1.4	...	6.3	7.0	7.3	7.6	...
Load keeping time /min	2	2	...	2	2	2	2	...

2.2. Experiment results and analysis

2.2.1. Failure mode analysis

A wheel coupler scaffold socket may be subjected to positive and negative bending moments because of its special structural form. The positive and negative failure modes of the socket were comprehensively analyzed. Fig. 6 shows the failure modes of the socket under a positive bending moment.

(a) P-SJ1

(b) P-SJ2

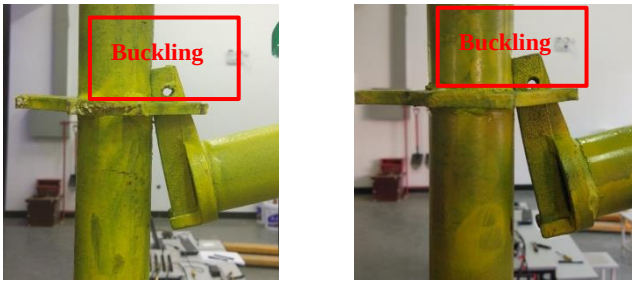

(c) P-SJ3 (d) P-SJ4

Fig. 6 Failure modes of various specimens (as listed in Table 1) in the positive direction

Fig. 6 shows that the socket in a bending state under a positive bending moment. A fracture occurred in P-SJ1 when the bending moment reached the ultimate value. No fractures occurred in P-SJ2, P-SJ3, and P-SJ4 when the bending moment reached the ultimate value. Based on the data listed in Table 1, we find that the failure modes are related to the depth of the socket inserted into the template. This is because the L_2 value of P-SJ1 was higher than that of the other specimens, and the higher the L_2 value, the easier it was for the socket to fracture. All the specimens underwent buckling at the contact position between the socket and the vertical post surface; however, the state of the socket determined the positive-direction bending capacity.

Fig. 7 shows the failure modes of the socket under a negative bending moment.

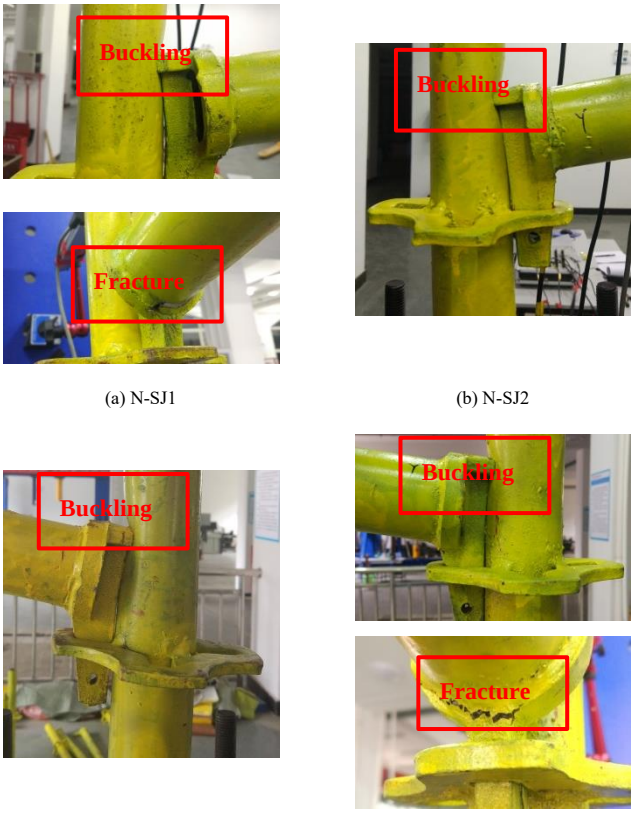

(a) N-SJ1 (b) N-SJ2

(c) N-SJ3 (d) N-SJ4

Fig. 7 Failure modes of various specimens (as listed in Table 1) in the negative direction

The failure modes of the N-SJ1 and N-SJ4 specimens were mainly fracture failure at the connection between the socket and the horizontal bar. The failure modes of N-SJ2 and N-SJ3 were mainly buckling of the vertical post. From the failure modes, we find that the negative-direction failure mode was different from the positive-direction failure mode, which was related to the depth of the socket inserted into the template and the material properties of the vertical post.

2.2.2. Bending capacity analysis

The moment–rotation angle curve was plotted by processing the data obtained from the positive-direction and negative-direction experiments. As shown in Fig. 8, the positive-direction bending capacity is largely the same at a bending moment of 0.45 kN·m; however, the initial bending stiffness in the positive direction is different, mainly because of the different L_2 values. Moreover, the negative-direction bending capacity is significantly different from the positive-direction bending capacity because of the different failure modes. The negative initial bending stiffness was unaffected by the L_2 value. By comparing the bending moment–rotation angle curves of N-SJ1 and N-SJ4, we find that the reduction in the bending stiffness was due to the initial imperfections of the vertical post. The negative-direction bending capacity and initial bending stiffness were much higher than those in the positive direction.

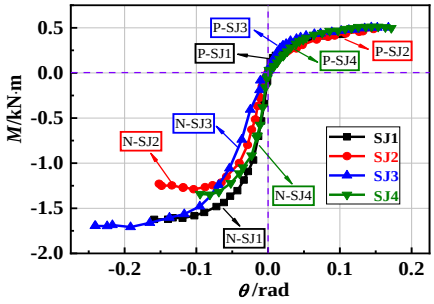

Fig. 8 Bending moment–rotation angle curve obtained experimentally

2.2.3. Constitutive model of material

Three standard arc specimens were prepared by randomly selecting a steel pipe, on which a tensile test was conducted to obtain its material properties. In accordance with the relevant requirements of GB/T 228.1-2010 “Metallic materials Tensile testing, Part 1: Method of test at room temperature” [31], the experimental specimen was prepared on the basis of the relevant requirements specified in appendix E.1, as shown in Fig. 9(a).

Assuming that the constitutive models of the horizontal bar and the vertical post are the same, the stress–strain curves of three groups of specimens are shown in Fig. 9(c). The yield strength was set to 256 MPa, and the elastic modulus was set to 2.02×10^5 MPa.

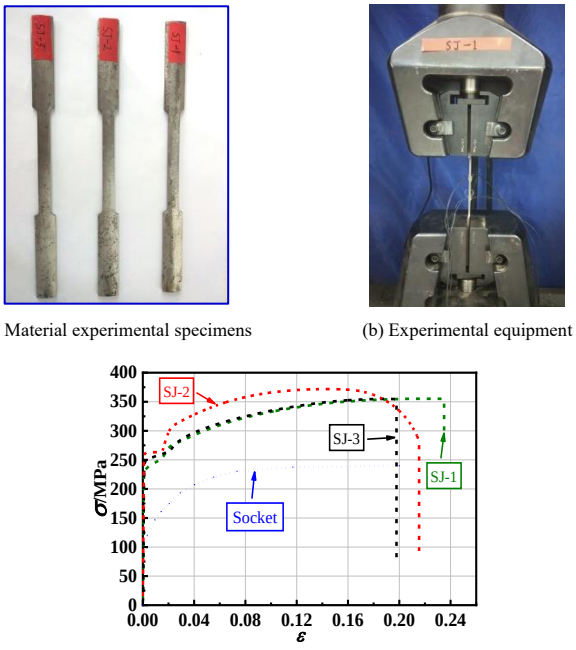

(a) Material experimental specimens (b) Experimental equipment

(c) Constitutive model of steel pipe and socket

Fig. 9 Constitutive model of material

The constitutive model of cast steel for the socket is also shown in Fig. 9(c). The constitutive model of the socket was obtained from existing literature given the difficulty in carrying out tensile tests on cast steel.

2.2.4. Verification and division of semi-rigid joints

Du [32] introduced and provided judgment criteria for the semi-rigid joint

of socket-type formwork supports when summarizing the domestic division of such joints, as shown in Fig. 10.

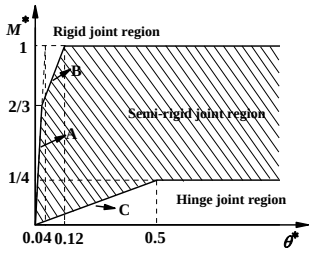

Fig. 10 Semi-rigid judgment criteria for socket-type joints

The curves in the figure were plotted using the following formula:

$$A: M^* \le 2/3, M^* = 25\theta^*;$$

$$B: 2/3 < M^* \le 1, M^* = (25\theta^* + 4)/7;$$

$$C: M^* = 0.5\theta^*。$$

$$M^* = M/M_p;\quad \theta^* = \theta/\left(M_p L_b / EI_b\right);$$

$$W_{px} = \frac{\pi}{4}(R^3 - \frac{r^4}{R});\quad I_b = \frac{\pi}{4}(R^4 - r^4).$$

Here, M_p represents the full plastic bending moment of the beam, $M_p = W_{px} \cdot f_y$, where W_{px} represents the plastic section modulus; EI_b/L_b represents the linear stiffness of the beam. I_b represents the cross-sectional moment of inertia.

The section size of the steel pipe was set to D48 mm × δ3.0 mm. E = 2.02×10^5 MPa, L_b = 0.3 m, and f_y = 256 MPa.

According to the above formula, it can be concluded that M_pL_b/EI_b = 0.01531 rad, and M_p = 1.150 kN·m.

The joint experimental data can be dimensionless–processed by the above formula, and then a curve can be drawn to divide the semi-rigid joint region, as shown in Fig. 11.

The connection joints of the wheel coupler-type formwork were typical semi-rigid connection joints based on the dimensionless bending moment–rotation angle curves of the four groups of joint experimental data shown in Fig. 11. As shown, they tend to the boundary of the hinge joint region when the joints are in the positive bending state and tend to the boundary of the rigid joint region when the joints are in the negative bending state.

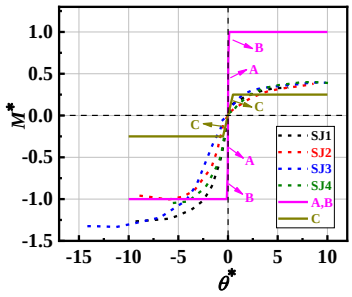

Fig. 11 Region division of semi-rigid joints

2.3. Finite element numerical analysis and verification

2.3.1. Establishing a finite element model

The finite element software ANSYS was used to establish a 3D solid model. The outer diameter and wall thickness of the steel pipe were set to 48 mm and 3.0 mm, respectively. Based on the experimental results of the material properties, the elastic modulus was set to 2.02×10^5 MPa, the Poisson's ratio was set to 0.3, the density was set to 7.85×10^{-6} kg/mm^3, and the empirical value of the friction coefficient was set to 0.2.

A refined finite element model was established in ANSYS to analyze the bending behavior of the socket connection. As shown in Fig. 12, the Solid185 element is discretized into a geometrical model, and the mesh size is set to 3.0 mm. The rigid beam scheme of MPC184 element was used to establish the loading points at both ends of the vertical post. The rigid beam scheme was used to connect the loading point with the node at the end of the steel pipe. As shown in Fig. 13, a displacement constraint is applied directly at the loading point. As shown in the red box in Fig. 13, the three translational degrees of freedom are constrained at the end of the horizontal bar. The translational degrees of freedom in the X and Y directions of the loading point were constrained at the upper end of the vertical post, and the translational degrees of freedom in the Y direction of the loading point was constrained at the lower end of the bar. The bending moment was applied by applying a displacement D in the X direction at the loading point at the lower end of the vertical post. Finally, the moment–rotation curve of the socket connection was obtained.

(a) Overall finite element model (b) CONTA174 element (c) TARGE170 element

Fig. 12 Numerical model of the socket connection

The contact elements CONTA174 and TARGE170 were used to simulate the mechanical behavior of the socket and the template, respectively, as shown in Figs. 12(b) and (c). The contact pair represents the contact and sliding between the socket element surface defined by CONTA174 and the deformable surface defined by TARGE170. The friction coefficient of the contact element was set to 0.2, and the normal stiffness was set to 1.0.

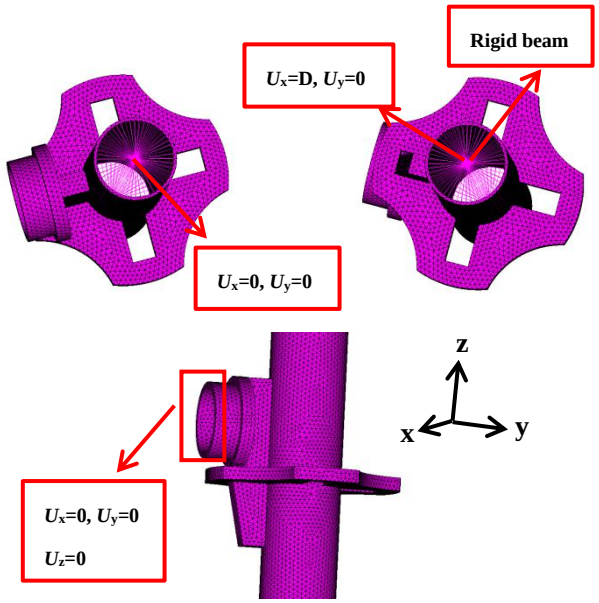

Fig. 13 Restraint condition of FE model

2.3.2. Comparative analysis of bending behavior

The results of the finite element model simulation were compared with the experimental results, as shown in Fig. 14. The finite element model can accurately predict the bending stiffness and bearing capacity in the positive direction. The finite element model can also effectively predict the bending stiffness in the negative direction. However, the finite element model cannot accurately predict the bending capacity of the socket when a fracture occurs in the experiment. Through the above results, we can verify the reliability of the finite element model in predicting the bending behavior of the connection joints of the wheel coupler-type formwork support.

For the case where the finite element results were not completely consistent with the experimental results, the failure modes of the joints in the positive and negative directions, shown in Figs. 5 and 6, indicate differences in the main components of the joints of the wheel coupler-type formwork support. When the joint was subjected to a bending moment, fracture failure easily occurs at the socket, at the connection of the socket and the horizontal

bar. The fracture failure occurs before the buckling failure of the joints. In which case, the finite element method cannot accurately simulate the buckling behavior of the joints.

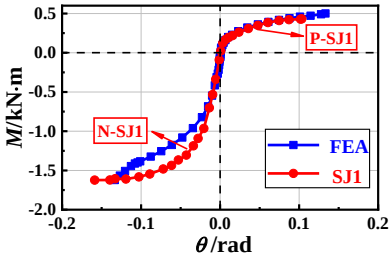

(a) SJ1

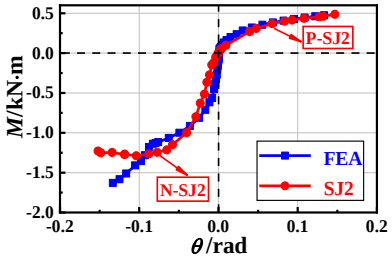

(b) SJ2

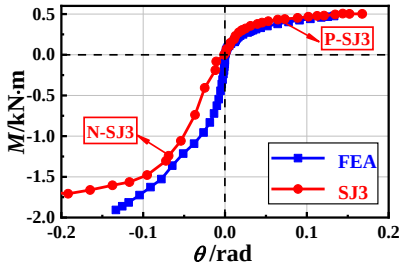

(c) SJ3

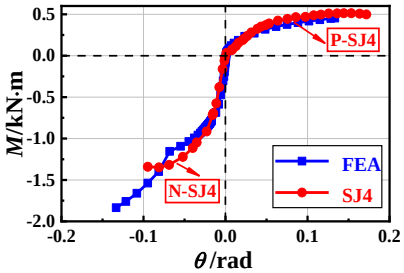

(d) SJ4

Fig. 14 Moment–rotation angle curves obtained from finite element simulation and experiments

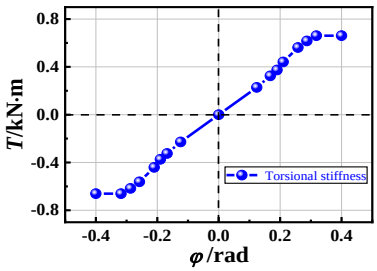

Fig. 15 Curve of torsion stiffness

2.3.3. Determination of the torsional stiffness of the socket connection

The finite element analysis software was used to analyze the torsional stiffness because the torsional stiffness of the socket connection of the wheel coupler-type formwork support cannot be accurately measured in the experiment. The complete torsional stiffness curve was obtained after analysis and processing using the same loading method as that employed for the bending stiffness, as shown in Fig. 15.

3. Parametric analysis of buckling behavior of wheel coupler-type high-formwork support system with diagonal bracing

3.1. Establishment of a finite element model

The key problem in establishing a finite element model in our study was accurately simulating the mechanical behavior of the semi-rigid socket connection. A nonlinear spring element COMBIN39 was used to simulate the bending behavior of the socket connection. The moment–rotation angle curves of SJ4 were set as the real constant of the COMBIN39 element. In addition, the "CP" command in ANSYS was used to couple the translational degrees of freedom of the nodes belonging to the horizontal bar and the vertical pole. Fig. 16(a) shows the finite element model of the socket connection. The torsion stiffness data can be analyzed through the finite element analysis results shown in Fig. 15, and the overall wheel coupler-type high-formwork support model was established using ANSYS, as shown in Fig. 16(b). The horizontal bar and vertical pole were simulated using the BEAM188 element, and the diagonal bracing was simulated using the LINK180 element. Generally, a high-formwork support system was used to bear the gravity load of the floor in construction engineering, so an overall uniform bearing load was set in the analysis, as shown in Fig. 16(c). In this section, two conditions were considered because the setting of the wall connecting pole was not always considered in actual engineering: with and without the application of a lateral constraint at the top, as shown in Fig. 16(d). First, an eigenvalue buckling analysis was carried out, and the first-order buckling mode was used as the initial geometrical imperfections. For the formwork support structure, 1/1000 of the total height was adopted as the initial imperfection [26, 27], which is a relatively conservative value in engineering. The initial imperfection value was set to H/1000, where H is the total height of the formwork support. Subsequently, a nonlinear buckling analysis of the overall formwork support was carried out to obtain the buckling coefficient. The critical load was the product of the buckling coefficient and the loading value. In this section, the buckling coefficient was used to represent the critical load. The greater the buckling coefficient, the greater the critical load, the greater the ultimate bearing capacity, and the better the overall stability. Otherwise, the worse. The magnitude of the applied load was P_w = 125.2 kN.

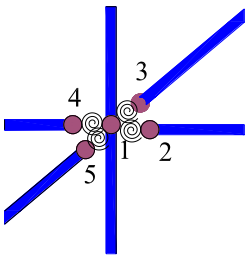

(a) Detailed connection of the FE model

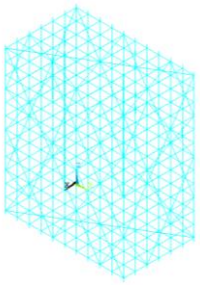

(b) Finite element analysis model

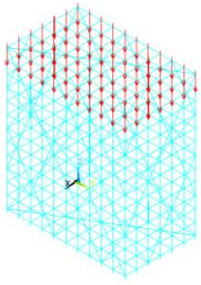

(c) Loading method

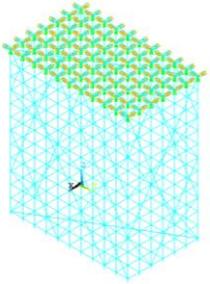

(d) Finite element analysis model with lateral constraints at the top

Fig. 16 Overall FE model

3.2. Influence of spatial layout of the diagonal bracing

Based on the specification requirements, a vertical diagonal bracing should be arranged at definite intervals along the span length in a high-formwork support system, and the vertical diagonal bracing should be arranged parallel to the short-side and long-side directions. A frame with 10×6×12 spans in the length, width, and height directions, respectively, was taken as the research object, l = w = h = 1.2 m, i.e., the transverse distance, longitudinal distance, and lift height were set to 1.2 m. The height of the frame H = 14.4 m, the width B = 7.2 m, and the aspect ratio H/B = 2 < 3, which meets the specification requirement. The plane layout of the vertical diagonal bracing has 4 spans × 6 steps. The angle between the diagonal bracing and the horizontal plane was set to 56.3°, and vertical and horizontal diagonal bracings were arranged around and up and down the frame, respectively. Fig. 17 shows the layout of the frame.

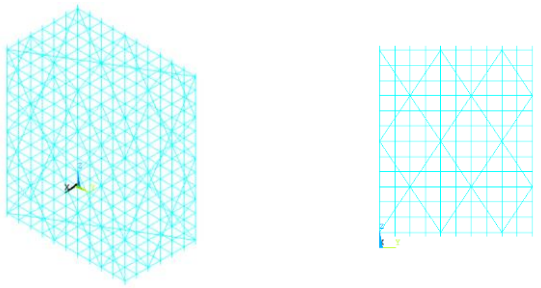

(a) Stereogram (b) Front view

Fig. 17 Layout of a 10×6×12 frame

The internal vertical diagonal bracing was arranged parallel to the short-side direction, at nine different intervals: every 1 span, every 2 spans, every 3 spans, every 4 spans, every 5 spans, every 6 spans, every 7 spans, every 8 spans and every 9 spans. When arranging parallel to the long-side direction, five intervals were considered: every 1 span, every 2 spans, every 3 spans, every 4 spans and every 5 spans. Fig. 18 shows the buckling coefficients under different conditions.

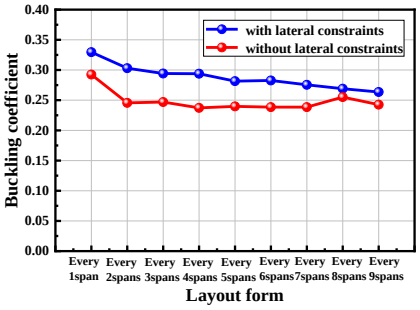

(a) Vertical diagonal bracing was arranged parallel to the short-side direction

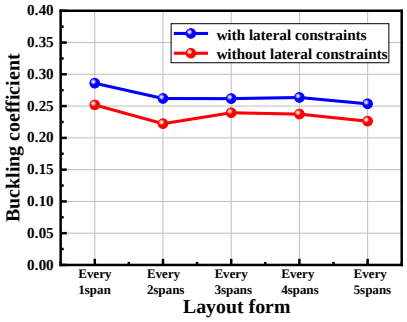

(b) Vertical diagonal bracing was arranged parallel to the long-side direction

Fig. 18 Variation in the buckling coefficients of a vertical diagonal bracing under different conditions

In summary, a comprehensive layout in which internal vertical diagonal bracings were arranged every 3 spans parallel to the short-side direction and every 3 spans parallel to the long-side direction was adopted to obtain the variation in the buckling coefficient with and without lateral constraints, as listed in Table 4.

Table 4
Variation in the buckling coefficient under parallel long- and short-side layouts of the vertical diagonal bracing

No:	Parallel short-side: every 3 spans	Parallel long-side: every 3 spans	Parallel long- and short-side: every 3 spans	Variation of buckling coefficient
With lateral constraints	0.294188	0.261688	0.320950	9.10%/ 22.65%
Without lateral constraints	0.247000	0.239500	0.257000	4.05%/ 7.31%

From Table 4, we find that the superposition layout has no significant influence on the overall stability. Therefore, considering the comprehensive economy, the internal vertical diagonal bracing can be arranged in the parallel short-side direction.

3.3. Influence of a plane layout of the vertical diagonal bracing

Currently, a large formwork system with 8×8×12 spans in the length, width, and height directions was taken as the research object, l = w = h = 1.5 m, i.e., the transverse distance, longitudinal distance, and lift height were set to 1.5 m. The height of the frame was 18 m, the width B = 12 m, and the aspect ratio H/B = 1.5 < 3, which meets the specification requirements. The vertical diagonal bracing was arranged only around the frame, whereas the horizontal diagonal bracing was arranged along the height direction of the frame every 6 steps. Six different layouts of the vertical diagonal bracing were studied: 2-span 2-step, 2-span 4-step, 2-span 6-step, 4-span 4-step, and 4-span 6-step. Fig. 19 shows the plane layout of the vertical diagonal bracing.

The buckling coefficient was obtained by a nonlinear buckling analysis of the six layouts and then compared with the buckling coefficient of the layout without the diagonal bracing. Table 5 presents the variation in the buckling coefficient.

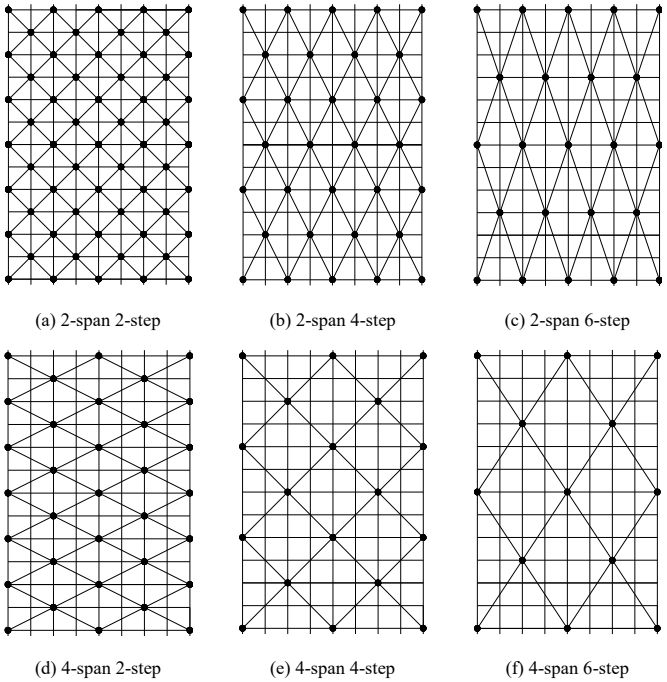

(a) 2-span 2-step (b) 2-span 4-step (c) 2-span 6-step

(d) 4-span 2-step (e) 4-span 4-step (f) 4-span 6-step

Fig. 19 Layout diagrams of the vertical diagonal bracing

Table 5
Comparison of buckling coefficients of different layouts of the vertical diagonal bracing

No:	Layouts of the vertical diagonal bracing	Number of joints on one side	Angle	Buckling coefficient with lateral constraints	Variation of buckling coefficient	Buckling coefficient without lateral constraints	Variation of buckling coefficient
	Without diagonal bracing			0.158562	0.00%	0.157400	0.00%
a	2×2	59	45°	0.223250	40.80%	0.191688	21.78%
b	2×4	32	63°	0.214980	35.58%	0.177000	12.45%
c	2×6	23	72°	0.207625	30.94%	0.179500	14.04%
d	4×2	33	27°	0.205950	29.89%	0.197200	25.29%
e	4×4	18	45°	0.199500	25.82%	0.185750	18.01%
f	4×6	13	56°	0.193763	22.20%	0.170750	8.48%

From the above table, we find that the overall stability of the high-formwork support system with a diagonal bracing was mainly affected by the joint density between the diagonal bracing and the frame, and the angle between the diagonal bracing and the horizontal plane. Next, two influencing factors were mainly explored.

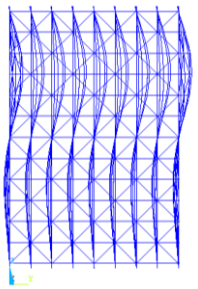

(a) With lateral constraints; 2-span 2-step

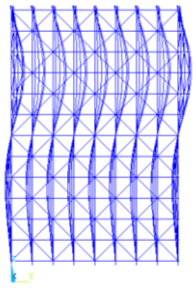

(b) Without lateral constraints; 2-span 2-step

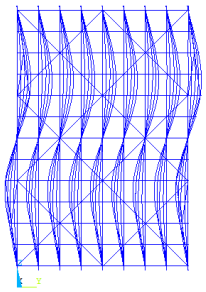

(c) With lateral constraints; 4-span 4-step

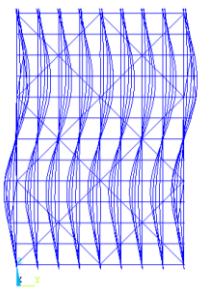

(d) Without lateral constraints; 4-span 4-step

Fig. 20 First-order buckling modes for different layouts of the vertical diagonal bracing

As shown in Fig. 20, the buckling modes of the integral formwork support in different plane layouts are bounded by the horizontal plane of the intermediate horizontal diagonal bracing. Large-wave drumbeating occurs both above and below the middle horizontal plane, and there were also conditions where large-wave drumbeating occurs above the middle horizontal plane. The deformation wavelength was related to the joint density between the diagonal bracing and the frame, and the angle between the diagonal bracing and the horizontal plane.

3.4. Influence of joint density between the diagonal bracing and the frame

To better study the influence of the joint density between the diagonal bracing and the frame on the overall stability, a series of numerical models with different joint densities were established under the same angle and height settings, and a nonlinear buckling analysis was carried out. In this section, we mainly study the numerical model of the formwork support system with two specifications, one with l = w = h = 1.5 m and the other with l = w = h = 1.2 m. Each specification has five conditions: a joint density of 27°, a joint density of 45°, a joint density of 56°, a joint density of 63°, and a joint density of 72°, as shown in Fig. 21.

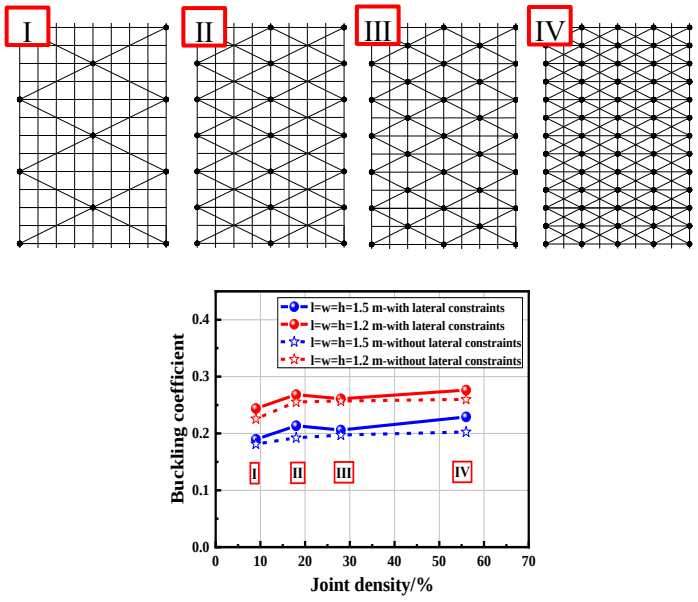

(a) 27°

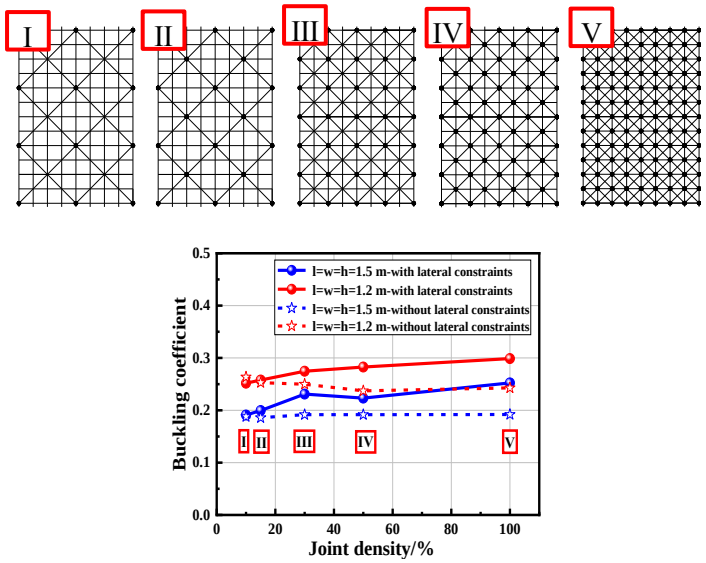

(b) 45°

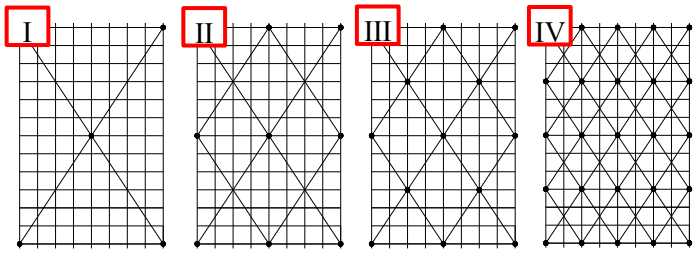

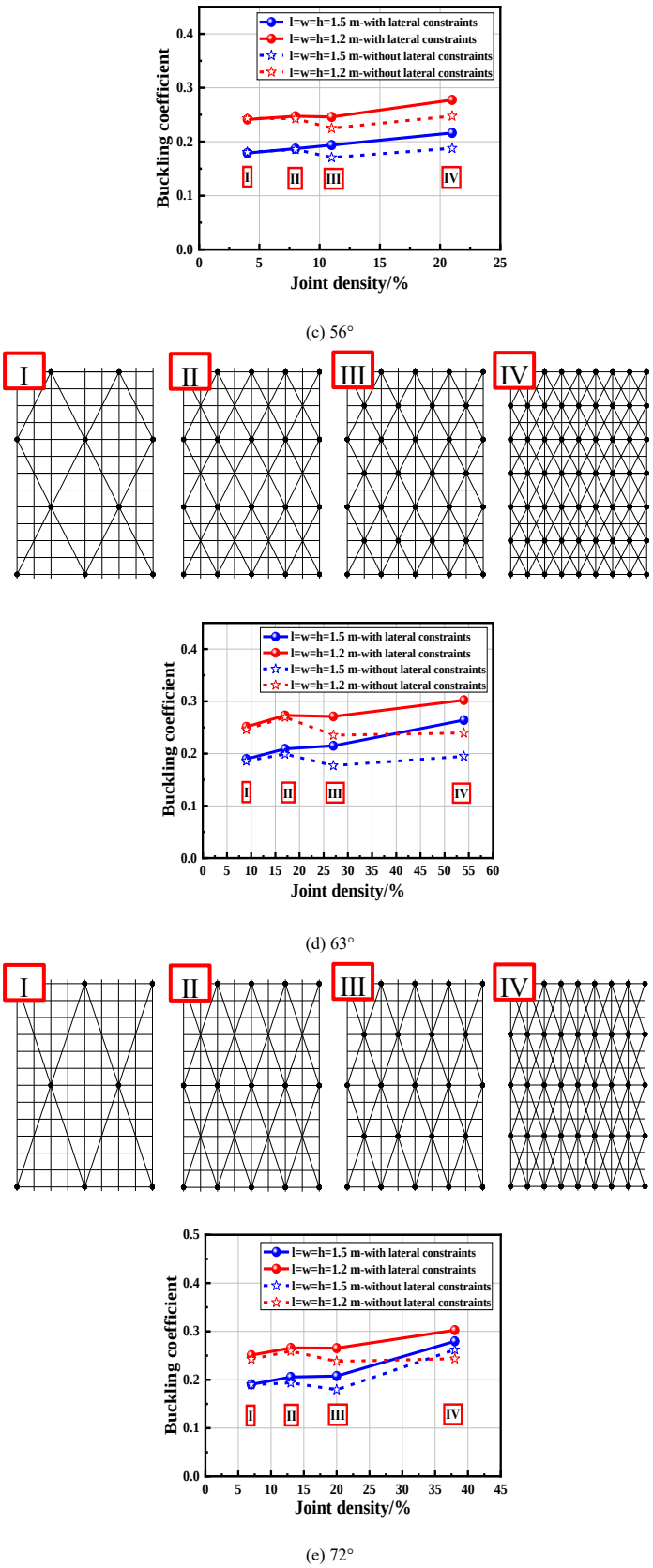

(c) 56°

(d) 63°

(e) 72°

Fig. 21 Comparison of buckling coefficients at different joint densities

The above analysis shows that with the increase in the joint density, nonlinear buckling coefficient increases gradually and that the overall stability improves while keeping the angle unchanged. However, this trend was not very evident, and the regularity was more evident when considerably increasing the joint density. From an economic perspective, an appropriate joint density connection form should be selected in the construction process.

We summarize the buckling coefficients corresponding to the joint density under five conditions of the same vertical diagonal bracing plane layout with two sizes to better illustrate the variation in the overall stability with the increase in the joint density under the same angle and vertical diagonal bracing plane layout. Fig. 22(a) shows the results in the condition of a lateral constraint at the top. Fig. 22(b) shows the results for the condition without any lateral constraints.

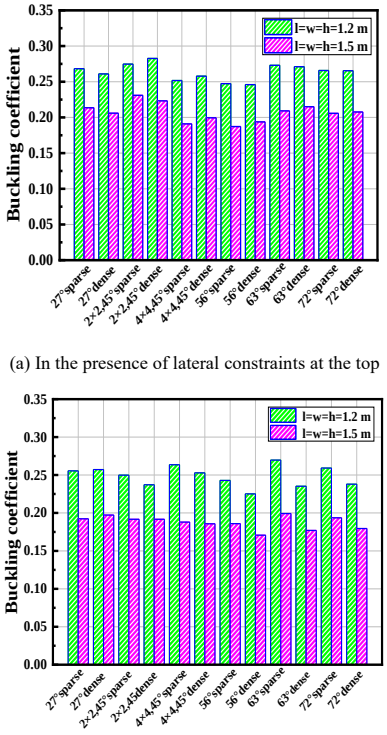

(a) In the presence of lateral constraints at the top

(b) In the absence of lateral constraints at the top

Fig. 22 Comparison of sparse buckling coefficients of the joints with and without lateral constraints at different angles and in the same layout

In summary, the higher the joint density, the better the overall stability in the presence of a lateral constraint at the top; the angle between the diagonal bracing and the horizontal plane and the layout of the vertical diagonal bracing were the same. From an economic perspective, a low joint density can meet the overall stability requirement.

Taking the high-formwork system with 8 spans × 8 spans × 12 steps as the research object, l = w = 1.5 m, the optimal plane layout and optimal angle were obtained with the variation in the lift height, as listed in Table 6.

Table 6
Optimal plane layout and optimal angle under different lift heights

Lift heights/m	Optimal plane layout	Optimal angle (°)	Optimal plane layout	Optimal angle (°)
0.3	2 spans, 4 steps	22	2 spans, 6 steps	31
0.6	2 spans, 4 steps	39	4 spans, 4 steps	22
0.9	2 spans, 4 steps	50	4 spans, 4 steps	31
1.2	2 spans, 2 steps	39	2 spans, 2 steps	39
1.5	2 spans, 2 steps	45	4 spans, 2 steps	27
1.8	2 spans, 4 steps	67	4 spans, 2 steps	31
2.1	2 spans, 2 steps	54	4 spans, 2 steps	35
2.4	2 spans, 4 steps	73	2 spans, 2 steps	58
3.0	2 spans, 4 steps	76	2 spans, 4 steps	76

With the increase in the lift height, the optimal angle increases when the lift height was small, and the optimal layout was a 2-span 4-step arrangement. With the increase in the lift height, the optimal angle increases steadily. The optimal plane layout was mostly a 2-span 4-step arrangement, though there were 2-span 2-step conditions as well. However, considering the comprehensive economy, the layout of the vertical diagonal bracing of a wheel coupler formwork support was a 2-span 4-step arrangement, and the optimal angle should be approximately in the range of 30–70°.

In the absence of a lateral constraint at the top, the optimal angle varies by approximately 30° when the lift height h was in the range of 0.3–2.1 m,

and the optimal angle was relatively large when the lift height h = 2.4 m and h = 3.0 m. The results show that the smaller the angle between the diagonal bracing and the horizontal plane, the better the overall stability in the absence of a lateral constraint at the top and when the lift height was not particularly large. The optimal angle was approximately 30°. The optimal plane layout cannot be determined, and the distribution was relatively random.

3.5. Influence of angle between the diagonal bracing and the horizontal plane

To better study the influence of the angle between the diagonal bracing and the horizontal plane on the overall stability at the top with and without a lateral constraint, the variation in the buckling coefficient at different angles was obtained, as listed in Table 7, for the same joint density but different lift heights.

Table 7
Comparison of buckling coefficients for the same joint density but different lift heights

Lift heights /m	Optimal plane layout	Number of joints on one side	Optimal angle (°)	Buckling coefficients with lateral constraints	Buckling coefficients without lateral constraints
0.3	4-span 2-step	33	6	0.695438	0.720438
	2-span 4-step	32	22	0.715950	0.716550
0.6	4-span 2-step	33	11	0.480950	0.455750
	2-span 4-step	32	39	0.498450	0.447000
0.9	4-span 2-step	33	17	0.328763	0.318875
	2-span 4-step	32	50	0.377313	0.314075
1.2	4-span 2-step	33	22	0.250125	0.234813
	2-span 4-step	32	58	0.255013	0.239075
1.5	4-span 2-step	33	27	0.205950	0.197200
	2-span 4-step	32	63	0.214980	0.177000
1.8	4-span 2-step	33	31	0.182000	0.166888
	2-span 4-step	32	67	0.193919	0.152625
2.1	4-span 2-step	33	35	0.167937	0.145437
	2-span 4-step	32	70	0.153650	0.135750
2.4	4-span 2-step	33	39	0.133406	0.124275
	2-span 4-step	32	73	0.161144	0.123250
3.0	4-span 2-step	33	45	0.104407	0.101844
	2-span 4-step	32	76	0.138250	0.109110

From Table 7, we find that in the presence of a lateral constraint at the top, the greater the angle between the diagonal bracing and the horizontal plane, the greater the buckling coefficient and the better the overall stability under the same joint density. In the absence of a lateral constraint at the top, the smaller the angle between the diagonal bracing and the horizontal plane, the greater the buckling coefficient and the better the overall stability under the same joint density.

4. Conclusions

The buckling behavior of a wheel coupler high-formwork support system with a diagonal bracing was systematically studied, and the positive and negative bending behaviors of the connection joints of the support were analyzed through experiments. A precise numerical model of the connection joints of the wheel coupler was established and verified through a finite element analysis. Based on the characteristics of the semi-rigid connections, the buckling behavior of the overall structure was analyzed. The influencing factors, such as the spatial layout of the diagonal bracing, the plane layout of the vertical diagonal bracing, the joint density between the diagonal bracing and the frame, and the angle between the diagonal bracing and the horizontal plane, were mainly studied.

1) The experimental results showed that the failure modes in the positive direction were relevant to the insertion depth of the socket into the template. The higher the L_2 value, the more likely the socket was to fracture. The failure modes in the negative direction were closely related to the insertion depth of the socket into the template and the bending of the vertical post.

2) The proposed moment–rotation curve was based on the same steel grade and component size. Further verification was required for different steel grades and component sizes. After dimensionless treatment of the experimental data, the dimensionless moment–rotation angle curve was plotted. The connection joint of the wheel coupler formwork support was a typical semi-rigid connection joint. Through a finite element analysis and parametric analysis, an accurate numerical model of the connection joint of the wheel coupler formwork support was established and verified.

3) Regardless of the application of a lateral constraint at the top, the internal vertical diagonal bracing should be arranged parallel to the short-side direction.

4) In the presence of a lateral constraint at the top, the optimal plane layout of the vertical diagonal bracing was found to be a 2-span 4-step arrangement, and the optimal angle was in the range of 30–70°. In the absence of a lateral constraint at the top, the optimal plane layout could not be determined, and when the lift height was moderate, the optimal angle was approximately 30°.

5) An appropriate joint density was conducive to the overall stability.

6) In the case of the same joint density, in the presence of a lateral constraint at the top, the higher the angle between the diagonal bracing and the horizontal plane, the better the overall stability. In the absence of a lateral constraint at the top, the smaller the angle between the diagonal bracing and the horizontal plane, the better the overall stability.

References

[1] Lu Z.R., “Experimental and theoretical study on fastener steel tube full hall formwork support system”, Tianjin: Tianjin University, 2010.
[2] Liu H.B., Zhao Q.H. and Wang X.D., et al, “Experimental and analytical studies on the stability of structural steel tube and coupler scaffolds without X-bracing”, Engineering Structures, 32(4), 1003-1015, 2010.
[3] Zhou K.Z., “Test and analysis on load-bearing capacity of steel tubular falsework with bowl-button-type connection”, Tianjin: Tianjin University, 2010.
[4] Dou G.J., Kang Y. and Zi J.T., et al, “Investigation and application analysis of socket type wheel-buckle scaffold”, Building Construction, 40(11), 1957-1958+1968, 2018.
[5] Chen M., “The study on the popularization and application of the pulley-clip high formwork in Wenzhou”, Hangzhou: Zhejiang University of Technology, 2016.
[6] Guangdong Provincial Bureau of Quality and Technical Supervision, Technical specification for safety of wheel-coupler steel tube scaffolding: DB44/T1876-2016, Guangdong, 2016.
[7] Zhao Z.W., Chen Z.H. and Yan X.Y., et al, “Simplified numerical method for latticed shells that considers member geometric imperfection and semi-rigid joints”, Advances in Structural Engineering, 19(4), 689-702, 2016.
[8] Abdel-Jaber M., Beale R.G., Shatarat N.K. and Shehadeh M.A., “Experimental and theoretical investigations of spigot connections under cyclic loading”, Advanced Steel Construction, 15(1), 37-46, 2019.

[9] Peng J.L., Wang S.H., Wang C.S. and Yang J.P., “Stability study on scaffolds with inclined surfaces and extended jack bases in construction”, Advanced Steel Construction, 17(1), 73-83, 2021.
[10] Zhao Z.W., Liu H.Q., Dong J.F. and Bian Y.X., “Buckling capacity of socket-template scaffold system without X-bracing”, Journal of Performance of Constructed Facilities, 34(1), 04019089: 1-14, 2020.
[11] Zhao Z.W., Liu H.Q., Liang B. and Yan R.Z., “Influence of random geometrical imperfection on the stability of single-layer reticulated domes with semi-rigid connection”, Advanced Steel Construction”, 15(1), 93-99, 2019.
[12] Chan S.L. and Zhou Z.H., “Second-order elastic analysis of frames using single imperfect element per member”, Journal of Structural Engineering, ASCE, 121(6), 939-945, 1995.
[13] Chan S.L. and Gu J.X., “Exact tangent stiffness for imperfect beam-column members”, Journal of Structural Engineering, ASCE, 126(9), 1094-1102, 2000.
[14] Chan S.L. and Cho S.H., “Second-order analysis and design of angle trusses Part I: Elastic analysis and design”, Engineering Structures, 30(3), 616-625, 2008.
[15] Cho S.H. and Chan S.L., “Second-order analysis and design of angle trusses, Part II: Plastic analysis and design”, Engineering Structures, 30(3), 626-631, 2008.
[16] Chan S.L., Huang H.Y. and Fang L.X., “Advanced anslysis of imperfect portal frames with semi-rigid base connections”, Journal of Engineering Mechanics, ASCE, 131(6), 633-640, 2005.
[17] Chan S.L. and Cho S.H., “Second-order P-Δ-δ analysis and design of angle trusses allowing for imperfections and semi-rigid connections”, Advanced Steel Construction, 1(1), 169-183, 2005.
[18] Chan S.L. and Chui P.P.T., “Non-Linear static and cyclic analysis of steel frames with semi-rigid connections”, Elsevier Science, 1999.
[19] Chen Z.H. and Zhao Z.W., “Analysis of door-type modular steel scaffolds based on a novel numerical method”, Advanced Steel Construction, 12(3), 316-327, 2016.
[20] Zhao Z.W., Liu H.Q. and Liang B., “Novel numerical method for the analysis of semi-rigid jointed lattice shell structures considering plasticity”, Advances in Engineering Software, 114, 208-214, 2017.
[21] Zhang Y.C., Design principle of steel structure, Beijing: Higher Education Press, 2004.
[22] Ye K., Zhao Y.Q. and Liu G., “The impact analyse between ultimate bearing capacity with semi-rigid node of fasteners template scaffold”, Journal of Civil, Architectural &Environmental Engineering, 37, 130-133, 2015.
[23] Liu H.B., Jia L. and Wen S.L., et al, “Experimental and theoretical studies on the stability of steel tube-coupler scaffolds with different connection joints”, Engineering Structures, 106, 80-95, 2016.
[24] Zou A.M., Li Q.W., He M.H. and Zhang H., “FEA on bearing behavior of cuplok scaffold based on tri-linear semi-rigid joint model”, Journal of Building Structures, 37(4), 151-157, 2016.
[25] Yang S., “The research on stability bearing capacity of wheel buckle steel tubular formwork support frame”, Changsha: Changsha University of Science & Technology, 2011.
[26] Yu W.K., Chung K.F. and Chan S.L., “Structural instability of multi-storey door-type modular steel scaffolds”, Engineering Structures, 26 (7), 867-881, 2004.
[27] Chu A.Y.T., Chan S.L. and Chung K.F., “Stability of modular steel scaffolding systems–theory and verification”, Advances in Building Technology, 1, 621-628, 2002.
[28] Sevim B., Bekiroglu S. and Arslan G., “Experimental evaluation of tie bar effects on structural behavior of suspended scaffolding systems”, Advanced Steel Construction, 13(1), 62-77, 2017.
[29] Liu H.B., Zhou Y., Chen Z.H. and Liu Q., “Structural performance and design method of new mortise–tenon full steel-tube scaffold”, Advanced Steel Construction, 14(2), 291-307, 2018.
[30] Qian X.J., “Experimental research and technical application of joint mechanical behavior of disk lock and cuplok steel tubular falsework”, Nanjing: Southeast University, 2016.
[31] Metallic materials–Tensile testing–Part 1: Method of test at room temperature: GB/T 228.1–2010. Beijing: China Standards Press, 2010.
[32] Du R.J., “Scientizing and standarding regulations on design and calculation of construction falsework in scaffold structure(2)”, Construction Technology, 39(2), 110-116, 2010.